Study of enhanced heat transfer performance of subcooled and saturated flow boiling with R365mfc on sintered porous coating high heat flux tubes

WANG, Ke, ZHANG, Qi, CHENG, Lixin, YANG, Junjun and YANG, Xu

Study of Enhanced Heat Transfer Performance of Subcooled and Saturated Flow Boiling with R365mfc on Sintered Porous Coating High Heat Flux Tubes

Ke Wang[a]*, Qi Zhang[a], Lixin Cheng[b]*, Junjun Yang[c], Xu Yang[c]

[a]Beijing Key Laboratory of Process Fluid Filtration and Separation, China University of Petroleum-Beijing, Beijing 102249, China

[b]Department of Engineering and Mathematics, Sheffield Hallam University, Sheffield S1 1WB, UK

[c]AT&M Environmental Engineering Technology Co., Ltd, Beijing 100080, China

∗Corresponding authors, e-mail: wang_ke@cup.edu.cn, lixincheng@hotmail.com

Abstract

Sintered porous coating tubes are high performance heat transfer components which are used to enhance boiling heat transfer. Sintering metal powder particles on the surfaces of plain tubes form porous coatings with numerous cavities which can promote nucleation of bubble generation in boiling processes and thus enhance boiling heat transfer enhancement. In the present study, experiments of the subcooled and saturated flow boiling heat transfer characteristics on the sintered porous coating tubes were conducted. The test tubes with porous coatings have an outer diameter of 25 mm, a length of 1 m and the coating thicknesses are 0.06 mm, 0.12 mm, 0.18 mm, and 0.25 mm, respectively. The heat transfer performance of high

flux tubes is evaluated with a mass flow rate ranging from 128.3 to 252.03 kg/m^2·s and the saturation temperature of the experimental section is controlled between 45-50℃. The influence of flow conditions, heat flux, and properties of the sintered layer on boiling heat transfer was discussed. The results indicate that sintered porous media can effectively reduce the degree of superheating required for boiling heat transfer, but they also inevitably increase in flow resistance. Remarkably, the heat transfer enhancement due to the porous media increases up to a certain point and then decreases, while the flow resistance increases as the sintered layers thicken. The maximum heat transfer coefficient of the sintered tube with a sintered thickness of 0.06 mm is 1.6 times greater than that of a smooth tube. However, increasing the thickness of the porous layer does not always enhance heat transfer. The effects of different particle sizes of the sintered grains and the thickness of the sintered layers under the conditions of subcooled boiling and the onset of nucleate boiling have been analyzed to understand the physical mechanisms. An empirical heat transfer correlation has been proposed according to the experimental results for the sake of design calculation in industry.

Keywords: Enhanced heat transfer, flow boiling, sintered porous coatings, high heat flux tube, bubble dynamics, mechanism, correlation

1. Introduction

Advanced heat transfer technologies and enhanced heat transfer techniques play a pivotal role in thermal, power, energy saving and storage, high heat flux removal, nuclear energy,

hydrogen production and utilization, automotive, mechanical engineering, aerospace engineering and environmental engineering etc. [1-4]. All attempts to achieving high efficiency, low emissions and low costs in various thermal processes and thermodynamic cycles include advanced heat transfer theory and knowledge, high performance heat transfer equipment and enhancement of heat transfer to a large extent. Shell-and-tube heat exchangers are commonly used in chemical engineering and many other relevant industries. Currently, heat exchangers predominantly utilize plain tubes, which are less efficient in terms of heat transfer, thereby exerting significant pressure on companies to achieve energy savings and emissions reductions. To enhance the flow boiling heat transfer of shell-and-tube exchangers such as reboilers and evaporators which involve phase change heat transfer of low boiling point fluids on external tubes, the strategy sintering metal particles onto the smooth surfaces of the tubes to increase the heat transfer area, creating artificial cavities for vaporization and strengthening the turbulence in the near-wall region to enhance heat transfer shows great promise as an intensified heat transfer technique.

High flux tubes are widely used in phase change equipment due to their excellent heat transfer capacity, such as in the evaporator, condenser, and reboiler. Plenty of artificial cavities are formed by sintering metal particles on the pipe surface to enhance phase-change heat transfer. Extensive research has been dedicated to the enhancement of heat transfer under pool boiling conditions using porous media. The impact of heating surface roughness on heat transfer has shown that an increase in surface roughness results in an elevated boiling heat transfer coefficient [5-9]. Porous media offers a greater number of cavities for boiling heat

transfer, which can enhance the heat transfer coefficient and augment the heat transfer capacity compared to a smooth surface [10-15]. Consequently, it can effectively mitigate the influence of temperature lag prior to boiling [16-20]. Furthermore, experimental studies have concentrated on the material, size, and quantity of additives in metal particles. The findings suggest that the size of the metal particles significantly influences boiling heat transfer. The heat transfer coefficient diminishes when the metal particle size surpasses the bubble diameter. It has also been observed that porous media can effectively impede scaling on metal surfaces [21-24]. By simulating pool boiling on the surface of porous media, bubbles continuously form and detach at lower levels of superheat, agitating the liquid pool and intensifying heat exchange [25, 26].

Sintered porous coating high heat flux tubes are distinguished by the composite powder sintered onto the plain tube substrate, altering the surface condition of the boiling surfaces. The inter-particle voids form pores that serve as centers for nucleate boiling, thereby transforming film boiling into nucleate boiling and significantly increasing the boiling heat transfer coefficient, effectively enhancing the heat transfer efficiency of evaporators, condensers, and reboilers. The porous layer on the tube surface has interconnected cavities, ensuring that bubbles can grow and detach from the pores as they absorb heat within the porous layer, while liquid flows into the porous layer through connecting tunnels surrounding the pores, resulting in a continuous process of intensified heat transfer. In general, high-flux tubes have the following advantages [21-26]:

- Higher heat transfer coefficient: The overall heat transfer coefficient for high-flux

tubes is 2 to 4 times higher than that of plain tubes.

- Lower boiling superheat: Capable of producing intense nucleate boiling at minimal wall superheat, the necessary wall superheat for boiling is only 1/7 to 1/8 that of plain tubes.
- Higher performance-price ratio: The improved heat transfer efficiency leads to reduced equipment size, lowering both the capital investment and the associated construction costs, thus offering a higher cost-performance ratio.
- Stronger anti-fouling capability: Due to the porous surface of the tubes, the circulation of fluid in the near-wall region is 10~15 times greater than that of plain tubes. The substantial liquid circulation acts to clean the surface of the tubes, granting them a higher resistance to fouling and less susceptibility to coking.

Compared to the research pool boiling and flow boiling inside tubes, research into flow boiling on the sintered porous coating high heat flux tubes is relatively limited. Based on the available literature on flow boiling [27-31], it has been found that surface modification can significantly amplify the boiling heat transfer coefficient, up to twice that of a plain tube. Furthermore, unlike the formation and detachment of bubbles in pool boiling, the primary force driving bubble departure shifts from buoyancy to shear force as the Reynolds number escalates [32-35]. Qin et al. [36] examined the dynamics of bubbles within the subcooled flow boiling process and offered an energy balance model and a force balance model for boiling bubbles during this process. They analyzed the changes in force during bubble growth and detachment and also demonstrated the application of bubble dynamics in boiling simulation. Additionally, Cheng and Chen [37] assessed several heat transfer correlations for flow boiling in tubes using experimental data.

According to the afore-going literature review, many studies of flow boiling inside high heat flux tubes have been conducted so far. However, studies of flow boiling on externally sintered porous coating high heat flux tubes are rare and limited. Therefore, research on enhanced flow boiling heat transfer on externally sintered high heat flux tubes is focused on in the present study. In order to understand the enhanced heat transfer characteristics and mechanisms of subcooled and saturated flow boiling point fluids on externally sintered porous coating high heat flux tubes, the heat transfer characteristics of single-phase, subcooled and saturated flow boiling with phase change in externally sintered porous coating high heat flux tubes with R365mfc were experimentally investigated. The effects of flow rate, superheat, and porous media thickness are analyzed. Furthermore, an empirical heat transfer correlation has been proposed based on experimental data. The novelty of the present study is to specifically address the impact of different particle sizes of the sintered grains and the thickness of the sintered layers under subcooled and saturated flow boiling conditions. By examining the conditions for the onset of nucleate boiling, it evaluates the degree of heat transfer enhancement of externally sintered porous coating tubes compared to plain tubes, thereby providing both theoretical and experimental foundations for externally sintered porous coating tubes.

2. Description of experimental system and data reduction methods

2.1 Experimental system

Figure 1 depicts the schematic of the test facility, which primarily comprises three circuits: (1) The heating circuit includes a reservoir, a centrifugal pump, a mass flow meter, a differential pressure transmitter, a test section, and temperature and pressure sensors arranged in and around the test section; (2) The condensing circuit cools the high-temperature two-phase fluid

in the test section. The loop includes a condenser, a cooling water source, and temperature sensors. Additionally, the bypass circuit regulates the flow of the heating loop using a ball valve. This valve allows for flow adjustment, ensuring experiment stability and safety. (3) The bypass circuit, equipped with a ball valve, regulates the flow of the heating loop. This valve enables flow adjustment, ensuring the stability and safety of the experiments. Considering the fixed quantity of refrigerant in the tank and the constant power of the pump, the flow rate can be adjusted by controlling the ball valve in the main circuit or altering the degree of openness of the ball valve in the bypass circuit.

The pressure drop is one of the key indicators for evaluating the performance of heat exchange components. In the heating circuit, differential pressure transmitters are utilized to capture the pressure drop across the porous medium surface of the high-flux tube, which arises due to the flow resistance encountered by the refrigerant. Furthermore, by measuring this differential pressure, the friction factor can be determined, thus allowing for an analysis of the impact that the sintered porous media has on flow resistance and phase change heat transfer. The high-temperature two-phase fluid is cooled through the condenser shown in the red box in Figure 1. The shell of the condenser is connected with the cooling water, and the pipe is connected with the two-phase fluid for convection heat transfer cooling.

Figure 2 illustrates the arrangement of sensors on the test section. The test section is a stainless steel shell equipped with an externally sintered high flux tube for testing purposes. The specific structure and size of the stainless-steel sleeve are shown in Figure 3. The test tubes with porous coatings have an outer diameter of 25 mm, a length of 1 m and the coating

thicknesses are 0.06 mm, 0.12 mm, 0.18 mm, and 0.25 mm, respectively. In the experiments, the refrigerant R365mfc is used as the working fluid, circulating through the annulus between the sleeve and the tube. The heat transfer performance of high flux tubes is evaluated with a mass flow rate ranging from 128.3 to 252.03 kg/m^2·s and the saturation temperature of the experimental section is controlled between 45-50℃. Table 4 lists the selected physical properties of the refrigerant R365mfc at atmospheric pressure. An electric heating rod, affixed to the inner wall of the high-flux tube, acts as the heat source, capable of delivering a heat flux of up to 3.5 kW/m² to the liquid. To ensure heat transfer efficiency, the gap between the heating rod and the pipe wall is filled with thermal conductive silicone grease. In addition to the temperature sensors installed at the inlet and outlet of the pipeline, four equidistant temperature sensors were employed to measure the pipe wall temperature, and three equidistant sensors were utilized to gauge the fluid temperature in the test section. Remarkably, a thermal feedback sensor is installed to ensure the accuracy of the heating temperature. To mitigate heat loss during the experiment, the entire experimental section is wrapped with insulation cotton.

Figure 4 illustrates the typical high flux tube utilized for testing in the current study, along with the microscopic structure of the sintered layer. The metal particles are sintered onto the plain tube and exhibit a high resistance to detachment. The metallic particulate material used for sintering is an iron alloy, with an average particle diameter ranging from 56 to 60 μm. The geometric parameters and dimensions of the test tube are detailed in Table 1. Currently, the propensity for delamination of sintered coatings is one of the primary factors that limit the development or industrial application of high-flux tubes. To ensure the implementation of flow

boiling tests, it is imperative that the sintered layer on the exterior of the test tubes remains intact throughout the experiment. Therefore, we commenced by conducting delamination resistance tests on the sintered layers of our test components. In this study, tubes featuring four distinct coating thicknesses were employed to assess the bonding strength of the coatings (as depicted in Figure 5). Conventionally, an average stress of 15 N is required to dislodge the sintered porous medium layer. Based on the findings of the coating stripping resistance test, as presented in Table 2, the high flux tubes utilized in this experiment satisfy the requisite strength criteria.

2.2 Data reduction methods

In the present study, the heat flux q can be obtained with the following equation:

$$q = \frac{\eta E}{A} \tag{1}$$

where E is the heating power, A is the area of heating surface, and η represents the heat loss efficiency in the experiments, which is determined through a heat balance test performed prior to each experiment. It is calculated using the following formula:

$$\eta = \frac{(h_{\text{out}} - h_{\text{in}})G}{E} \tag{2}$$

where h_{out}, h_{in} and G denote the enthalpy values of the R365mfc at the outlet and inlet of the test section and liquid mass flow rate, respectively. The heat balance test results reveal that complete elimination of heat dissipation is unattainable, even with substantial insulation applied to the test section. Furthermore, accounting for the thermal resistance due to conduction, the heat balance test suggests that the thermal efficiency for the present experiment is approximately 0.9. The parameters E and A are determined by the following equations:

$$E = UI \tag{3}$$

$$A = \pi DL \tag{4}$$

where U is the input voltage, I is the current, D is the diameter of the heat exchange tube and L is the length of heat exchange tube.

The average heat transfer coefficient of the experimental section k is determined by Newton's law of cooling, which states that the heat flux q is proportional to the temperature difference ΔT.

$$k = \frac{q}{\Delta T} \tag{5}$$

$$\Delta T = T_{\mathrm{wavg}} - T_{\mathrm{favg}} \tag{6}$$

where T_{wavg} represents the average temperature of the tube wall, and T_{favg} is the average temperature of the fluid in the test section.

As the fluid flows through the annulus between the sleeve and the tube, the mass flux M can be calculated as:

$$M = \frac{G}{A_s} \tag{7}$$

$$A_s = \frac{1}{4}\pi(D_s + D)(D_s - D) \tag{8}$$

where A_s and D_s are the annular chamber area and the inner diameter of the sleeve, respectively.

In the present study, the thermodynamic vapor quality x is employed to evaluate the phase change.

$$x = \frac{h_{\mathrm{f}} - h_{\mathrm{l}}}{h_{\mathrm{gl}}} \tag{9}$$

where h_{f} is the fluid enthalpy, h_{l} is the saturated liquid enthalpy corresponding to the test pressure, and h_{gl} is the latent heat of vaporization of the liquid corresponding to the test pressure.

Note that the thermodynamic vapor quality is applicable exclusively to single-component mixture (e.g. refrigerant with steam in the present study) and can take values x < 0 for sub-cooled fluids. In the present study, the vapor qualities x at measurement location z were calculated from heat balances based on heat flux q as follows [37]:

$$x(z) = \frac{\pi(D_S - D)(z - L_{sub})q}{MA_s h_{gl}} \tag{10}$$

where L_{sph} is the length of the single phase inlet region, which can be determined by:

$$L_{sph} = \frac{MA_s c_p(T_{sat} - T_{in})}{\pi(D_S - D)q} \tag{11}$$

where c_p is constant-pressure specific heat of fluid, T_{sat} is the saturation temperature of boiling, and T_{in} is the temperature of the fluid flowing into the test section. Additionally, The Reynolds number Re, Nusselt number Nu, and Prandtl number Pr are respectively defined as:

$$Re = \frac{\rho V(D_s - D)}{\mu} \tag{12a}$$

$$Nu = \frac{h(D_s - D)}{\lambda} \tag{12b}$$

$$P_r = \frac{c_p \mu}{\lambda} \tag{12 c}$$

where ρ is liquid density, V is the liquid velocity, μ is the dynamic viscosity of liquid, λ is thermal conductivity.

Since the experimental study focuses on enhancing boiling heat transfer in horizontal porous sintered tubes, the effects of gravity on pressure drop can be ignored. The pressure drop in the test section for single-phase flow includes both frictional pressure drop and pressure losses at the inlet and outlet. The total pressure drop can be expressed as follows:

$$dP_t = dP_f + dP_m \tag{13}$$

where dP_t, dP_f and dP_m are total pressure drop, friction pressure drop, and pressure loss at the inlet and outlet, respectively. The pressure loss at the inlet and outlet can be calculated using the following formula.

$$dP_m \approx 1.5\left(\frac{V^2}{2v}\right) \tag{14}$$

where V is the flow velocity of the working medium, and v is the specific volume of the working medium. Thus, the friction pressure drop can be obtained as:

$$dP_f = dP_t - dP_m \tag{15}$$

The friction factor f is commonly used to characterize the frictional resistance in a flow channel and can be calculated by:

$$f = \frac{2dP_f D_s}{\rho L_{\text{eff}} v^2} \tag{16}$$

where L_{eff} is the effective flow length.

To assess the augmentation of heat transfer in high flux tubes, both sintered high flux tubes and plain tubes are utilized to investigate the impact of porous media on boiling heat transfer. In this study, the liquid mass flux varies from 128.30 to 252.03 kg/m²·s, maintaining the saturation temperature of the working fluid within the experimental section at a range of 45-50°C. For each experimental run, fluctuations in temperature and pressure gradient are meticulously recorded at a sampling rate of 1000 Hz over a duration of 60 seconds. It is important to note that all experiments are performed under atmospheric pressure conditions.

2.3 Measurement uncertainties

The flow rate of the liquid is determined using a vortex flow meter, which possesses an uncertainty of 0.1%. Pressure measurements are conducted with an SD-802 pressure

transmitter, featuring an uncertainty of 0.5%. The pressure drop across the test section is gauged using a Rosemount 3051 differential pressure transmitter, which boasts an accuracy of 0.04%. Temperature measurements are performed with a PT100 sensor, achieving an accuracy of ±0.3 K.

Additionally, the errors in the measured parameters of *k*, *x*, *Re*, and *Nu* can be calculated according to the error analysis method described in references [38] and [39]. The maximum uncertainty for each calculation result is presented in Table 3.

$$\delta k = \sqrt{\left(\frac{q}{\left(\mathrm{T}_{\mathrm{wavg}} - T_{\mathrm{favg}}\right)^2}\left(\delta T_{\mathrm{wavg}} - \delta T_{\mathrm{favg}}\right)\right)^2} \tag{17}$$

$$\delta_{L_{\mathrm{sub}}} = \sqrt{\left(\frac{A_{\mathrm{s}} c_p (T_{\mathrm{sat}} - T_{\mathrm{in}})}{\pi (D_s - D) q}\Delta M\right)^2 + \left(\frac{M A c_p}{\pi (D_s - D) q}\left(\Delta T_{\mathrm{sat}} - \Delta T_{\mathrm{in}}\right)\right)^2} \tag{18}$$

$$\delta_x = \sqrt{\left(-\frac{\pi (D_S - D) q}{M A_s h_{gl}}\Delta L_{sub}\right)^2 + \left(-\frac{\pi (D_S - D)(L - L_{sub}) q}{A_s h_{gl} M^2}\Delta M\right)^2} \tag{19}$$

$$\delta Re = \sqrt{\left(\frac{d}{\mu}\delta M\right)^2} \tag{20}$$

$$\delta Nu = \sqrt{\left(\frac{d}{\lambda}\delta k\right)^2} \tag{21}$$

3 Experimental results and discussion

3.1 Pressure drop

There is no doubt that the presence of porous media invariably leads to an increase in flow resistance due to augmented surface roughness. Figure 6 illustrates the relationship between pressure drop and flow rates in both plain and sintered tubes, the latter having varying

thicknesses of the sintered porous layer. Additionally, the relationship between the friction factor and Reynolds number under adiabatic conditions is illustrated in Figure 7. It can be deduced that the pressure drop is directly proportional to the thickness of the porous layer. Notably, the data on the variation of pressure drop with mass flux challenges prior assumptions, revealing that the pressure drop escalates with increasing flow rate. This unexpected phenomenon could potentially be ascribed to the roughness on the external surface of the tubes. The plain tube used in this study is not hydraulically smooth and exhibits significant surface roughness (Ra = 46 μm). According to the Moody chart [40], within the transitional turbulent zone, the friction factor along the flow path is influenced by both the Reynolds number and the relative roughness of pipe. In this zone, the friction factor increases with the Reynolds number. Moreover, in this experimental context, as the fluid traverses the annular space, the behavior of the friction factor as a function of the Reynolds number exhibits a deviation from that seen in traditional pipe flow. In the case of high-flux tubes, the incorporation of a sintered porous layer significantly enhances the roughness of tube surface, which intensifies with increasing coating thickness. As the thickness of the porous medium increases, the sintering process forms a metal skeleton structure that enhances the turbulence of the fluid flowing through the channels. As a result, the friction factor continues to increase. However, the influence of the thickness of sintered metal on the friction pressure drop decreases as turbulence in the test section increases. Furthermore, diverging from experiments that involve water flow within tubes, this study employs refrigerant R365 as the working fluid, which circulates through the annulus. Consequently, the distinctive properties of the fluid and the flow cross-section

configuration might also play a role in the observed discrepancies between the results of this study and the previously established understanding.

3.2 Subcooled flow boiling heat transfer

The primary advantage of a high-flux tube is its ability to minimize the superheat required for boiling, i.e., the ability to initiate boiling at an earlier stage is crucial in evaluating the performance of a high-flux tube compared to a plain tube. This early onset of boiling (ONB) can lead to improved heat transfer efficiency and overall performance of the heat exchange system. Therefore, it is necessary to study the properties of subcooled boiling heat transfer in sintered high-flux tubes.

Figure 8 illustrates the variation of vapor quality with different featured tubes in subcooled boiling region. The vapor quality decreases with an increase in the Reynolds number, and when the liquid mass flux reaches a certain level (M > 182.62 kg/m²·s in the present study), the thermodynamic equilibrium quality becomes negative. This indicates that the boiling flow transitions from saturated flow boiling to subcooled flow boiling.

Figure 9 illustrates the relationship between vapor quality and the heat transfer coefficient during subcooled boiling heat transfer. The heat transfer coefficients of both porous and smooth pipes show a trend proportional to vapor quality. Notably, the enhancement in heat transfer is closely related to the thickness of the sintered layer. Compared to plain tubes, an artificial cavity with a thickness of 0.06 mm significantly enhances heat transfer. However, as the thickness of the sintered layer increases, this effect gradually diminishes. When the thickness of the sintered

layer exceeds 0.18 mm, the heat transfer performance of the porous tube is unexpectedly worse than that of the plain tube. As the thickness of the sintered layer on high-flux tubes increases, it inevitably raises the resistance encountered by bubbles as they detach from the wall surface. When the degree of superheat reaches a certain level, a substantial number of bubbles are generated within the porous medium. However, due to the resistance imposed by the porous structure, these bubbles may not be swept away from the wall by the fluid in a timely manner. This leads to the coalescence of numerous bubbles within the porous medium, resulting in the formation of a vapor film, which significantly reduces the heat transfer coefficient of the high-flux tubes. Therefore, although increasing the thickness of the porous medium can enlarge the number of cavities and thereby increase the quantity and frequency of bubble formation, it also enhances the resistance faced by the bubbles during escape.

Figure 10 illustrates the relationship between the thickness of the sintered layer and the superheat required for boiling. When the heat flux is low, ΔT_{sat} is negative, indicating that natural convection heat transfer dominates in subcooled boiling. According to the experimental data, the heat transfer enhancement decreases as the thickness of the porous layer increases under subcooled conditions. It is speculated that the flow of liquid through the thicker porous layer is restricted due to the lower permeability of the sintered layer.

As illustrated in Fig. 11, the smooth surface of the tube is sintered to form a porous medium, allowing liquid to promptly fill the pores through capillary action, thus generating a higher number of active nucleation sites (cavities). Simultaneously, the direction of capillary force aligns with the concavity of the surface, that is, towards the center of the tube's diameter.

The synergistic action of capillary forces and buoyancy serves as the primary mechanism to ensure that bubbles grow upwards and detach from the wall. Note that reducing the surface energy of the fluid is necessary to enhance its wettability when flowing over a rough surface. Occasionally, some of the liquid may become trapped in the corners of the pores. When the wall surface is heated, the internal pressure of the remaining liquid in the pores increases. This increase in pressure promotes a phase change and leads to the formation of bubbles in the cavities. When the combined forces of internal pressure and buoyancy exceed the resistance of the rough surface, bubbles continuously detach from the wall surface. Meanwhile, due to capillary action, the pores are immediately refilled by the surrounding liquid.

Figure 11 depicts the force analysis of bubble growth and detachment. Bubbles that form on the surface of a plain tube are primarily influenced by various factors such as the external fluid pressure (F_d), internal pressure (F_p) caused by bubble expansion when heated, as well as the viscous force and surface tension of the outer liquid, which are collectively referred to as F_s. The metastable equilibrium state of the bubble can be calculated using the Clapeyron-Clausius equation, which is based on the principle of equal free energy.

$$\frac{\mathrm{d}p}{\mathrm{d}T} = \frac{h_g - h_l}{v_g - v_l} = \frac{h_{gl}}{\Delta v T_s} \tag{21}$$

where T_s, h_g, h_l, v_g and v_l are saturation temperature, gas phase entropy, saturated liquid phase entropy, specific volumes of gas and liquid phase, respectively.

For a spherical bubble, the metastable state of the force on the bubble can be obtained as follows:

$$F_p - F_d = \frac{2\sigma}{R} \tag{22}$$

where σ is the liquid surface tension coefficient, and R is the bubble radius, which can be determined by:

$$R = \frac{2\sigma T_s}{h_{gl}\rho_g \Delta T_s} \tag{23}$$

where ΔT_s is the superheat required to produce bubbles during boiling heat transfer.

As the driving force for the departure of bubbles, the upward buoyancy force under metastable equilibrium conditions can be obtained as:

$$F_b = (\rho_l - \rho_g) g v_b \tag{24}$$

where v_b and g are the bubble volume and gravitational acceleration, respectively.

Accordingly, the condition for bubble departure can be described as:

$$F_p + F_b > \frac{2\sigma}{R} \frac{\rho_l}{(\rho_l - \rho_g)} + F_d \tag{25}$$

For sintered high-flux tubes with porous media, more efficient artificial cavities are created. Thus, the capillary force F_r generated in the pores should be taken into consideration. As shown in Figure 11, as the thickness of the sintered layer increases, the single pore becomes elongated. At this stage, the resistance of the sintered skeleton F_w to bubble evolution increases, and the influence of the capillary force F_r can be ignored. Accordingly, the heat transfer capacity during boiling is inversely proportional to the thickness of the porous layer. The critical condition for bubble departure in porous media can be described as:

$$F_p + F_b + F_r > \frac{2\sigma}{R} \frac{\rho_l}{(\rho_l - \rho_g)} + F_d + F_w \tag{26}$$

Porous media not only provide more cavities for boiling heat transfer, but the capillary force within the porous media can also continuously activate these cavities. Additionally, the porous structure formed by sintering has a large surface area, increasing the heat transfer area

and, to some extent, enhancing the heat transfer process. By comprehensively analyzing the behavior of boiling bubbles and the unique structure of porous media, the relationship between the thickness of the porous layer and the subcooled boiling heat transfer coefficient is thoroughly examined, as depicted in Fig. 12.

During the dominant stage of subcooled boiling, it is evident that the subcooled boiling heat transfer coefficient of high-flux heat exchange tubes with a porous medium thickness of 0.06 mm is significantly higher than that of plain surface tubes. At this thickness, the maximum subcooled boiling heat transfer coefficient is 1.2 times that of plain surface tubes. However, increasing the thickness of the porous layer leads to a decrease in the heat transfer coefficient of subcooled boiling, an increase in flow resistance, and delayed detachment of small bubbles from the heating wall. Consequently, the heat transfer coefficient decreases.

3.3 Saturated flow boiling heat transfer

Under continuous heating by the electric heating rod, the working fluid in the experimental section transitions from subcooled boiling heat transfer to nucleate boiling heat transfer. During nucleate boiling heat transfer, the influence of porous media on heat transfer becomes more pronounced. Figure 13 illustrates the correlation between the vapor quality of the test section and the boiling heat transfer coefficient during nucleate boiling heat transfer. It can be observed that as the vapor quality of the test section increases, the boiling heat transfer coefficient also increases. Similarly, as the thickness of the porous medium increases, the resistance of boiling bubbles to detach from the heating wall also increases, affecting both the vapor quality and the heat transfer coefficient of the test section.

The relationship between superheat and surface heat flux of heat exchange tubes under nucleate boiling conditions is depicted in Figure 14. Under these conditions, the surface heat flux of an externally sintered high-flux heat exchange tube with a porous layer thickness of 0.25 mm is similar to that of a plain surface tube. This similarity is attributed to the special surface structure of the tube. However, the surface heat flux of porous tubes with different thicknesses is generally greater than that of plain surface tubes. In the nucleate boiling state, the maximum surface heat flux of a porous tube with a thickness of 0.06 mm is 1.6 times higher than that of a plain surface tube.

The internal storage of a significant amount of heat in the cavitation structure ensures that the working fluid rapidly reaches the boiling bubble state. However, an increase in the thickness of the porous medium prevents boiling bubbles from detaching promptly. It is speculated that this leads to a deterioration in local heat transfer on the surface of the tube with a thickness of 0.25 mm, resulting in a decrease in heat transfer efficiency.

The relationship between the superheat of the experimental section and the boiling heat transfer coefficient in the nucleate boiling state is illustrated in Figure 15. Analysis shows that in the nucleate boiling state, the highest boiling heat transfer coefficient is obtained from experiments conducted on porous tubes with a porous layer thickness of 0.06 mm. The maximum heat transfer coefficient is 1.6 times higher than that of a plain surface tube. In subcooled boiling heat transfer, the maximum heat transfer coefficient is 1.2 times higher than that of a plain surface tube. This indirectly indicates that sintered high-flux heat transfer tubes are more suitable for nucleate boiling heat transfer processes. In addition, it can be observed

that under lower superheat conditions, porous tubes can achieve nucleate boiling heat transfer more effectively. This suggests that the unique properties of the porous layer enhance the boiling heat transfer performance, particularly in the nucleate boiling regime.

3.4 Proposed heat transfer correlation

So far, there are no prediction methods available for flow boiling on sintered porous coating tubes in the literature. In order to meet the design calculation for industrial applications, a correlation between the thickness of the sintered layer and the heat transfer performance is proposed by incorporating several dimensionless numbers and base on the experimental data obtained in this study. The proposed correlation incorporates various dimensionless parameters, such as the Reynolds number (Re), Nusselt number (Nu), Prandtl number (Pr), and a dimensionless ratio (H/D) that characterizes the sintering thickness (H) in relation to the tube diameter (D). The Dittus-Boelter formula is commonly used to assess the effectiveness of single phase forced convection heat transfer. In this study, an original formula has been proposed to evaluate flow boiling heat transfer the high flux tubes. The formula is based on the Dittus-Boelter formula but takes into account the enhanced heat transfer of the porous layers. The formula can be expressed as follows:

$$Nu = 0.023Re^{0.8}Pr^{0.4} + (\frac{H}{D})^{a}Re^{b} \quad (27)$$

Figure 16 shows the empirical relationship curve that is fitted using experimental data collected from the test section at a heating temperature of 50℃. At the same time, the empirical relationship is modified, and different parameters, a and b, are obtained, respectively. The results are as follows:

$$a = \begin{cases} -2.67994, & \delta_1: 0.06\ mm \\ -2.67247, & \delta_2: 0.12\ mm \\ -2.50471, & \delta_3: 0.18\ mm \\ -2.31658, & \delta_4: 0.25\ mm \end{cases} \tag{28}$$

$$b = \begin{cases} -1.0835, & \delta_1: 0.06\ mm \\ -0.8315, & \delta_2: 0.12\ mm \\ -0.69109, & \delta_3: 0.18\ mm \\ -0.50695, & \delta_4: 0.25\ mm \end{cases} \tag{29}$$

By fitting the experimental data, the general prediction relation of flow boiling heat exchange performance of external sintered heat exchange tube can be expressed as follows:

$$Nu = 0.023Re^{0.8}Pr^{0.4} + (\frac{H}{D})^{-2.5879}Re^{-0.7553} \tag{30}$$

The proposed correlation is applicable to flow boiling heat transfer on sintered porous coating tubes for the purpose of industrial design calculation. However, the correlation needs to be improved to meet a wide range of conditions when more experimental data are available in future.

4 Conclusions

In the present study, an experimental investigation is carried out to examine the heat transfer characteristics of subcooled boiling in high-flux tubes. The study focuses on the impact of surface characteristics of externally sintered high-flux tubes on subcooled boiling heat transfer. Empirical relationships were derived to establish the correlation between these surface characteristics and the heat transfer process. The findings suggest a positive correlation between the thickness of the sintered layers and the increase in flow resistance, while the porosity remains constant. There is unequivocal evidence that a porous medium offers a greater number of cavities for enhanced heat transfer during boiling.

The heat transfer performance improves with a decrease in the thickness of the sintered layer; however, this improvement becomes restricted as the thickness of the layer increases. In the current investigation, it was observed that the sintered tube exhibited a maximum heat transfer coefficient that was 1.6 times greater than that of the plain tube. It is expected that the coalescence of bubbles in thicker sintered layers will lead to the formation of a vapor film, acting as a barrier between the heating wall and the surrounding liquid. This phenomenon will result in a decrease in the heat transfer coefficient.

Additionally, the effect of the sintered layers is characterized by a dimensionless number H/D. Based on the Dittus-Boelter formula and employing regression analysis, the present study proposes a modified formula for the assessment of porous high-flux tubes. This formula accounts for the enhanced heat transfer due to the porous layer and provides a comprehensive means of evaluating the heat transfer performance of high-flux tubes with various sintered layer thicknesses.

Acknowledgement

The authors gratefully acknowledge research support from the National Key Research and Development Program of China (No. 2023YFC2809004), National Natural Science Foundation of China (No. 52376157), Energy efficiency improvement research project of Sinopec (No. 320096).

NOMENCLATURE

A	area of heating surface, m^2	U	input voltage, V

A_s	annular chamber area, m^2	v_b	bubble volume, m^3
c_p	specific heat capacity, $J \cdot kg^{-1} \cdot °C^{-1}$	V	liquid velocity, $m \cdot s^{-1}$
D	tube diameter, mm	x	vapor quality
D_s	inner diameter of the sleeve, m	z	distance, m
E	heating power, kW	***Greek symbols***	
F_d	external fluid pressure, N	δ	thickness, mm
F_p	bubble internal pressure, N	η	experimental body thermal efficiency
F_s	interface surface tension, N	λ	thermal conductivity, $kW \cdot m^{-1} \cdot °C^{-1}$
F_w	resistance force exerted by the sintered skeleton, N	μ	dynamic viscosity, $Pa \cdot s$
g	gravitational acceleration, $m \cdot s^{-2}$	v	specific volumes
G	mass flow rate, kg/m^2	ρ	density, $kg \cdot m^{-3}$
h	enthalpy, kJ/kg	σ	liquid surface tension coefficient, $N \cdot m^{-1}$
h_{lg}	latent heat, kJ/kg		
I	current, A	***Subscripts***	
k	heat transfer coefficient, $kW \cdot m^{-2} \cdot °C^{-1}$	*avg*	average
L	length of heat exchange tube, m	*c*	cooling water
L_{sph}	single phase length of test section, m	*f*	fluid
L_{eff}	the effective flow length, m	*g*	gas
M	mass flux, $kg \cdot m^{-2} \cdot s^{-1}$	*in*	inlet
Nu	Nusselt number	*l*	liquid
		lg	liquid-gas
P	pressure, Pa	*out*	outlet

		sat	saturation
		sph	single phase
Pr	Prandtl number	*T*	tube
q	heat flux, kW·m^{-2}	*w*	wall
Q	heating power, kW		
R	bubble radius, m		
Re	Reynolds number		
s	entropy, kJ·℃$^{-1}$		
T	temperature, ℃		

References

[1] L. Cheng, K. Wang, G. Xia and A. J. Ghajar, Advanced heat transfer technologies: Fundamentals and applications, Heat Transfer Eng. 44 (21–22) (2023) 1947–1949.

[2] T. G. Karayiannis and M. M. Mahmoud, Flow boiling in microchannels: Fundamentals and applications, Appl. Therm. Eng. 15 (2017) 1372–1397.

[3] L. Cheng and D. Xia, Fundamental issues, mechanisms and models of flow boiling heat transfer in microscale channels, Int. J. Heat Mass Transf. 108 (Part A) (2017) 97-127.

[4] L. Cheng and G. Xia, Flow patterns and flow pattern maps for adiabatic and diabatic gas liquid two phase flow in microchannels: Fundamentals, mechanisms and applications, Exp. Therm. Fluid Sci. 148 (2023) 110988.

[5] H. Honda, H. Takamastu and J. Wei, Enhanced boiling of FC-72 on silicon chips with micro-pin-fins and submicron-scale roughness, J. Heat Transf. 2002, 124 (2) 383-390.

[6] J. Kim, S. Jun, R. Laksnarain and S. M. You, Effect of surface roughness on pool boiling heat transfer at a heated surface having moderate wettability, Int. J. Heat Mass Transf. 101 (2016) 992-1002.

[7] M. J. Tummers and M. Steunebrink, Effect of surface roughness on heat transfer in

Rayleigh-Benard convection, Int. J. Heat Mass Transf. 139 (2019) 1056-1064.

[8] J. S. Kim, A. Girard, S. Jun, J. Lee and S. M. You, Effect of surface roughness on pool boiling heat transfer of water on hydrophobic surfaces, Int. J. Heat Mass Transf. 118 (2018) 802-811.

[9] M. S. El-Genk and M. Pourghasemi, Experimental investigation of saturation boiling of HFE-7000 dielectric liquid on rough copper surfaces, Therm. Sci. Eng. Prog. 15 (2020) 100428.

[10] A. Kundu, R. Kumar, A. Gupta, Heat transfer characteristics and flow pattern during two-phase flow boiling of r134a and r407c in a horizontal smooth tube. Exp. Therm. Fluid Sci. 57 (2014) 344-352.

[11] A. Kundu, R. Kumar, A. Gupta, Comparative experimental study on flow boiling heat transfer characteristics of pure and mixed refrigerants. Int. J. Refrig. 45 (2014) 136-147.

[12] A. K. Dewangan, A. Kumar, R. Kumar, Experimental study of nucleate boiling heat transfer of R-134a and R-600a on thermal spray coating surfaces. Int. J. Therm. Sci. 110 (2016) 304-313.

[13] A. K. Dewangan, A. Kumar, R. Kumar, Nucleate boiling of pure and quasi-azeotropic refrigerants from copper coated surfaces. App. Therm. Eng. 94 (2016) 395-403.

[14] A. K. Dewangan, A. Kumar, R. Kumar, Experimental Study of Nucleate Pool Boiling of R-134a and R-410a on a Porous Surface. Heat Trans. Eng. 40 (2019) 1249-1258.

[15] A. K. Dewangan, A. Kumar, R. Kumar, Experimental study of bubble behaviors during boiling of a hydrocarbon refrigerant. Int. J. Therm. Sci. 166 (2021) 106989.

[16] M. S. El-Genk, Nucleate boiling enhancements on porous graphite and microporous and macro–finned copper surfaces, Heat Transfer Eng. 2012, 33 (3) 175-204.

[17] H. S. Jo, M.-W. Kim, T. G. Kim, S. An, H.-G. Park, J.-G. Lee, S. C. James, J. Choi and S. S. Yoon, Supersonically spray-coated copper meshes as textured surfaces for pool boiling, Int. J. Therm. Sci. 132 (2018) 26-33.

[18] H. S. Jo, T. G. Kim, J.-G. Lee, M.-W. Kim, H. G. Park, S. C. James, J. Choi and S.S. Yoon, Supersonically sprayed nanotextured surfaces with silver nanowires for enhanced pool boiling, Int. J. Heat Mass Transf. 123 (2018) 397-406.

[19] L. Lin and M. A. Kedzierski, Review of low-GWP refrigerant pool boiling heat transfer on enhanced surfaces, Int. J. Heat Mass Transf. 131 (2019) 1279-1303.

[20] S. K. Singh and D. Sharma, Review of pool and flow boiling heat transfer enhancement through surface modification, Int. J. Heat Mass Transf. 181 (2021) 122020.

[21] H. Jo, S. An and S. S. Yoon, Pool boiling enhancement by nanotextured surface of hierarchically structured electroplated Ni nanocones, Int. J. Heat Mass Transf. 173 (2021) 121203.

[22] M. Esawy, M. S. Abd-Elhady, M. R. Malayeri and H. Müller-Steinhagen, Influence of sintering on deposit formation during pool boiling of calcium sulphate solutions, Exp. Therm. Fluid Sci. 34 (2010) 1439-1447.

[23] W.-T. Ji, Z.-G. Qu, Z.-Y. Li, J.-F. Guo, D.-C. Zhang and W.-Q. Tao, Pool boiling heat transfer of R134a on single horizontal tube surfaces sintered with open-celled copper foam, Int. J. Therm. Sci. 50 (2011) 2248-2255.

[24] S. Jun, J. Kim, D. Son, H.Y. Kim and S.M. You, Enhancement of Pool Boiling Heat Transfer in Water Using Sintered Copper Microporous Coatings, Nucl. Eng. Technol. 48 (2016) 932-940.

[25] H. Li, R. Li, R. Zhou, G. Zhou and Y. Tang, Pool boiling heat transfer of multi-scale composite copper powders fabricated by sintering-alloying-dealloying treatment, Int. J. Heat Mass Transf. 147 (2020) 118962.

[26] S. Mori, F. Yokomatsu and Y. Utaka, Enhancement of critical heat flux using spherical porous bodies in saturated pool boiling of nanofluid, Appl. Therm. Eng. 144 (2018) 219-230.

[27] S. A. Khan, N. Sezer, S. Ismail and M. Koç, Design, synthesis and nucleate boiling

performance assessment of hybrid micro-nano porous surfaces for thermal management of concentrated photovoltaics (CPV), Energ. Convers. Manage. 195 (2019) 1056-1066.

[28] A. Arcasi, A. W. Mauro, G. Napoli and L. Viscito, Heat transfer coefficient, pressure drop and dry-out vapor quality of R454C. Flow boiling experiments and assessment of methods, Int. J. Heat Mass Transf. 188 (2022) 122599.

[29] Y. Y. Hsieh, Y. M. Lie and T. F. Lin, Saturated flow boiling heat transfer of refrigerant R-410A in a horizontal annular finned duct, Int. J. Heat Mass Transf. 50 (2007) 1442-1454.

[30] S. Xie, Q. Tong, Y. Guo, X. Li, H. Kong and J. Zhao, The effects of surface orientation, heater size, wettability, and subcooling on the critical heat flux enhancement in pool boiling, Int. J. Heat Mass Transf. 149 (2020) 119230.

[31] M. B. Darshan, Ravi Kumar and Arup Kumar Das, Numerical study of interfacial dynamics in flow boiling of R134a inside smooth and structured tubes, Int. J. Heat Mass Transf. 188 (2022) 122592.

[32] Y. Zhu, H. Hu, G. Ding, S. Sun and Y. Jing, Influence of metal foam on heat transfer characteristics of refrigerant-oil mixture flow boiling inside circular tubes, Appl. Therm. Eng. 50 (2013) 1246-1256.

[33] O. R. Alomar, M. A. A. Mendes, D. Trimis and S. Ray, Numerical simulation of complete liquid-vapor phase change process inside porous media: a comparison between local thermal equilibrium and non-equilibrium models, Int. J. Therm. Sci. 112 (2017) 222-241.

[34] S. Gong, P. Cheng, Lattice Boltzmann simulation of periodic bubble nucleation, growth and departure from a heated surface in pool boiling, Int. J. Heat Mass Transf. 64 (2013) 122-132.

[35] S. Gong, P. Cheng, Numerical investigation of saturated flow boiling in microchannels by the Lattice Boltzmann Method, Numer. Heat Transf. Part A. 65 (2014) 644–661.

[36] J. Qin, Z. G. Xu, Z. Y. Liu, F. Lu and C. Y. Zhao, Pore-scale investigation on flow boiling

heat transfer mechanisms in open-cell metal foam by LBM, Int. Commun. Heat Mass Transf. 110 (2020) 104418.

[37] L. Cheng, T. Chen, Comparison of six typical correlations for upward flow boiling heat transfer with kerosene in a vertical smooth tube, Heat Transfer Eng. 21(2000) 27-34.

[38] J. R. Taylor, W. Thompson, An introduction to error analysis: the study of uncertainties in physical measurements, Am. J. Phys. 51 (1997) 57-58.

[39] R. J. Mofat, Describing the uncertainties in experimental result, Exp. Therm. Fluid Sci. 01 (1988) 3-17.

[40] L. F. Moody, Friction factors for pipe flow. ASME Trans. 66 (1944) 671-684.

List of table captions

Table 1 Dimensions of the test high heat flux tubes.

Parameter	**Dimension**
Outer diameter of tube, D, m	0.025
Tube length, L, m	1
Tube thickness, δ_t, mm	3
Thickness of the sintered layer, δ_s, mm	0.06, 0.12, 0.18, 0.25

Table 2 Test of coating stripping resistance.

Thickness of sintered layer δ_s (mm)	Maximum stress of shedding (N)
0.06	20.13
0.12	21.94
0.18	23.19
0.25	24.47

Table 3. Measurement uncertainties.

Parameters	**Uncertainty**
Heat transfer coefficient, α	±7.8%
Subcooled length of test section. L_{sub}	±9.2%
Vapor quality, x	±13.8%
Reynolds number, Re	±2.8%
Nusselt number, Nu	±2.1%

Table 4. The selected physical properties table of R365mfc at atmospheric pressure.

Temperature (℃)	Density (kg/m³)	Enthalpy (kJ/kg)	c_p (kJ/kg·K)	Viscosity (μPa·s)	Phase
30	1246.3	240.77	1.3867	463.55	Liquid
32	1242.0	243.55	1.3908	451.85	Liquid
34	1237.6	246.34	1.3949	440.56	Liquid
36	1233.2	249.13	1.3990	429.66	Liquid
38	1228.8	251.93	1.4033	419.14	Liquid
40	1224.4	254.74	1.4075	408.97	Liquid
40.186	1224.0	255.01	1.4079	408.04	Liquid
40.186	6.0338	443.19	1.0441	9.9366	Vapor
42	5.9924	445.09	1.0464	9.9999	Vapor
44	5.9475	447.19	1.0491	10.070	Vapor
46	5.9034	449.29	1.0518	10.139	Vapor
48	5.8602	451.39	1.0546	10.209	Vapor
50	5.8177	453.50	1.0575	10.278	Vapor

List of figure captions

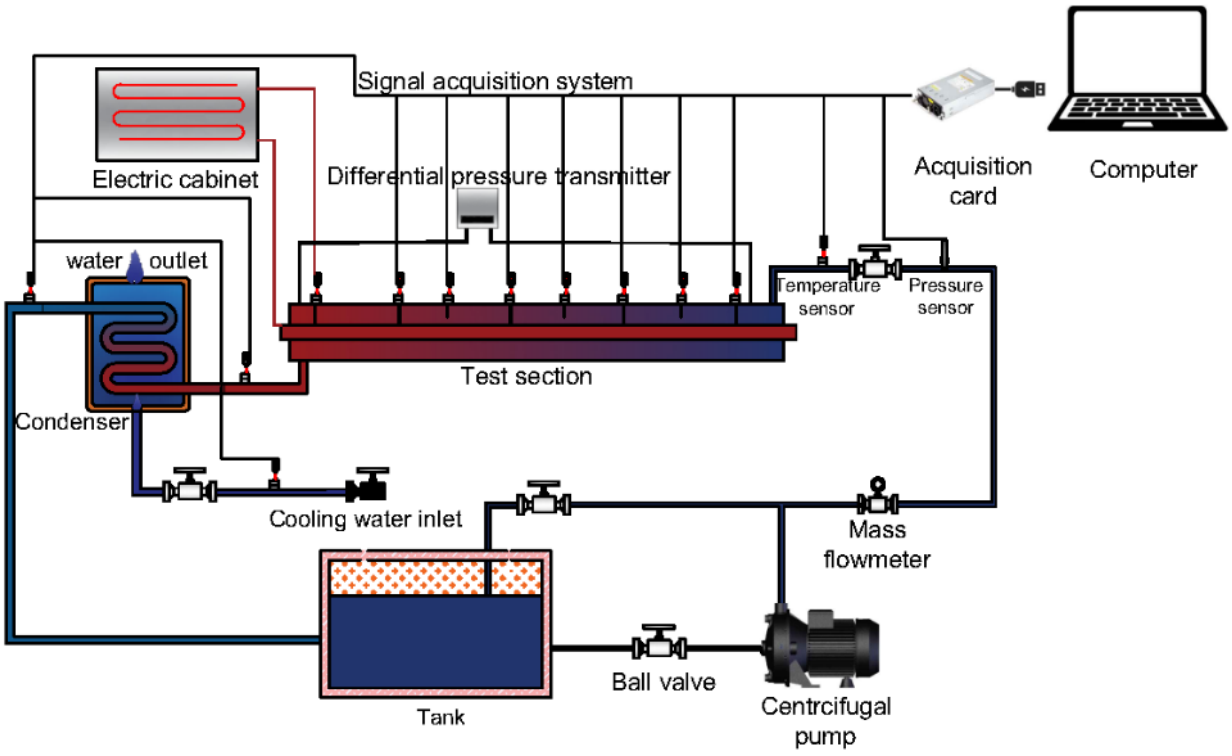

Figure 1. Schematic diagram of the experimental apparatus.

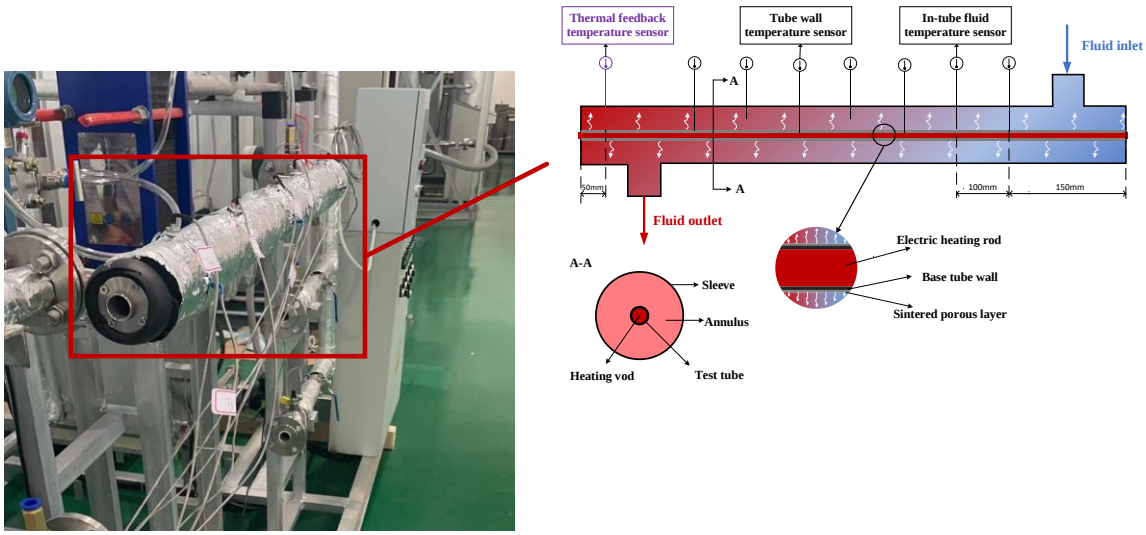

Figure 2. The arrangement of sensors on the test section.

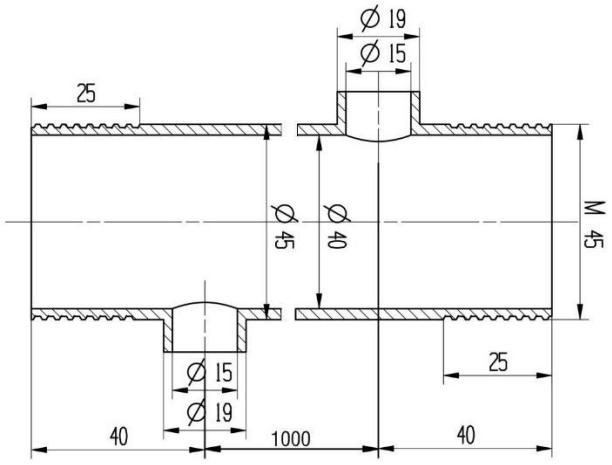

Figure 3. The specific structure and size of the stainless-steel sleeve.

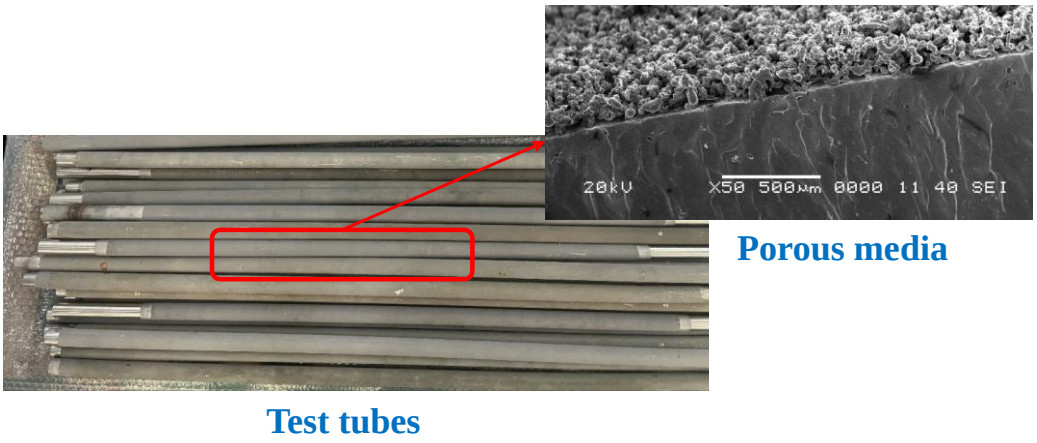

Figure 4. The macro and microstructure of the sintered high flux tubes.

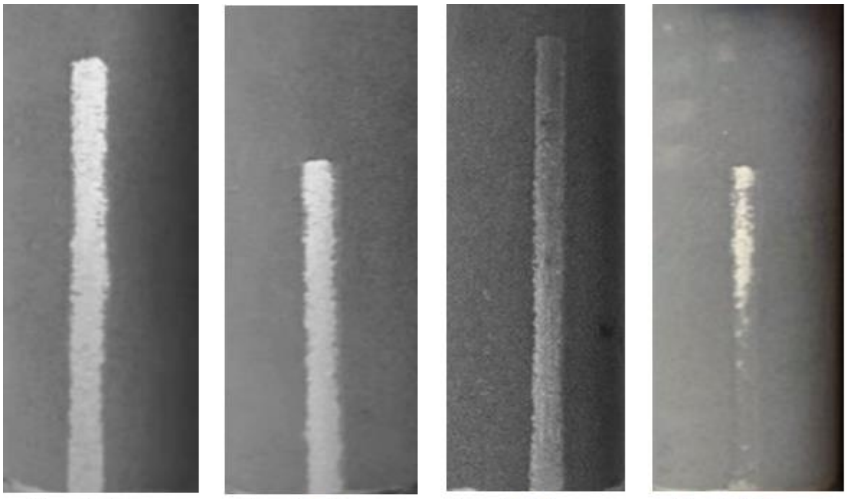

Figure 5. Bonding strength test of sintered layer.

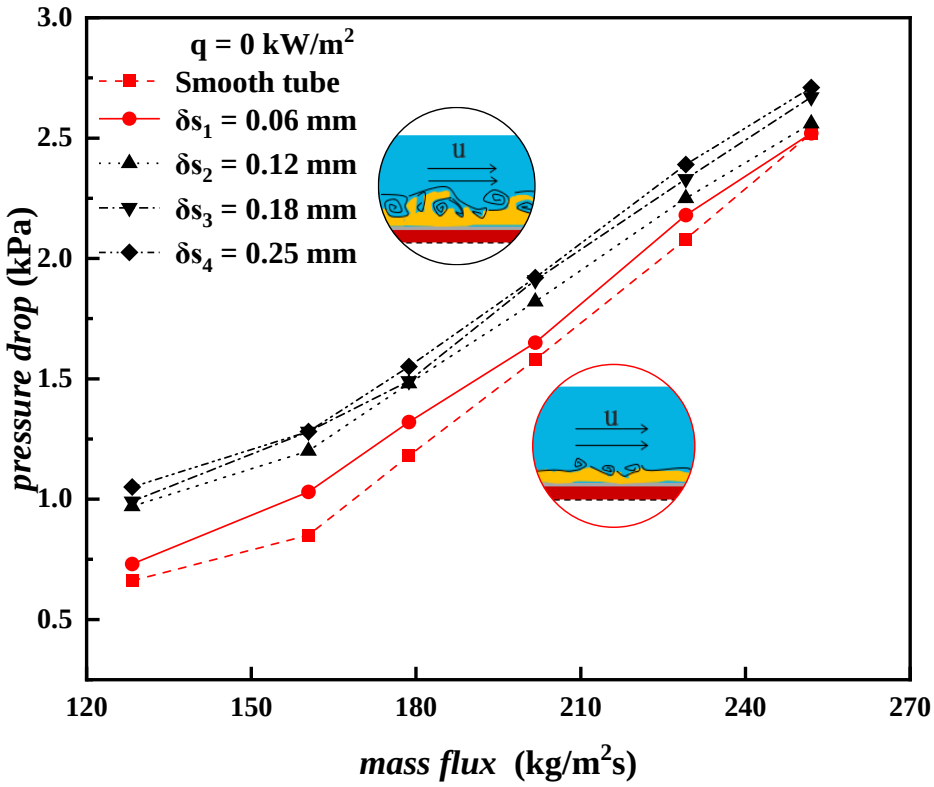

Figure 6. Variation of the pressure drop vs. mass flux under different flow conditions under adiabatic condition.

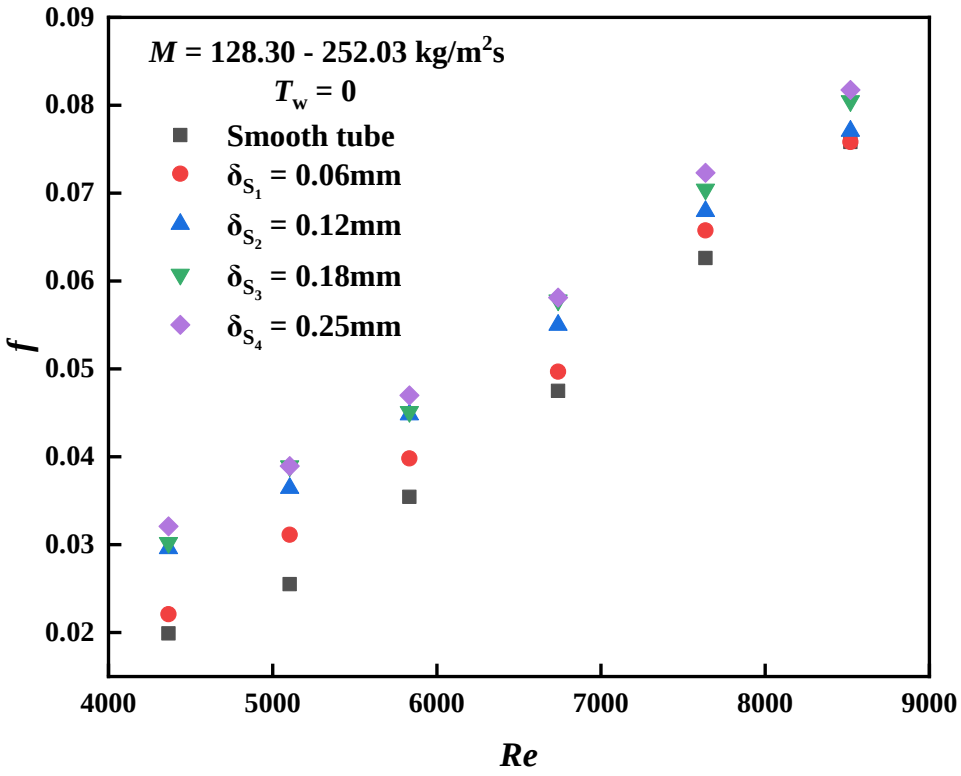

Figure 7. Variation of single-phase flow friction factor vs. Reynolds number.

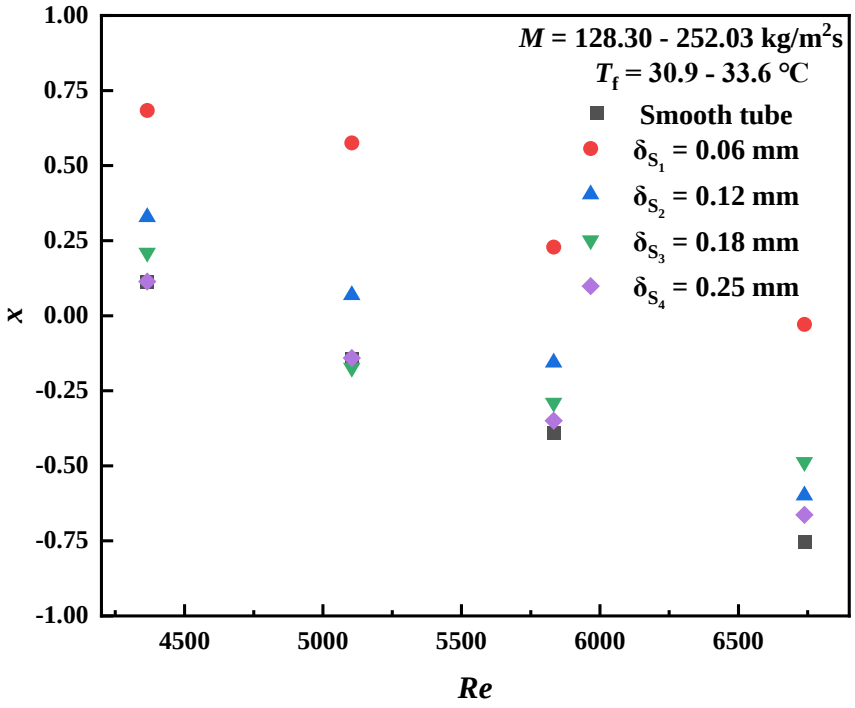

(a)

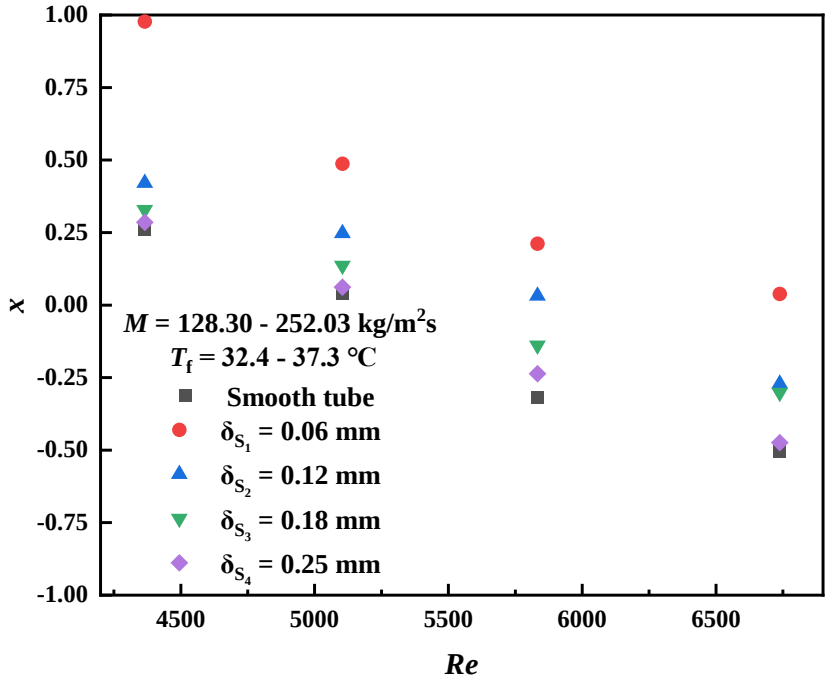

(b)

Figure 8. The relationship between vapor quality and Reynolds number.

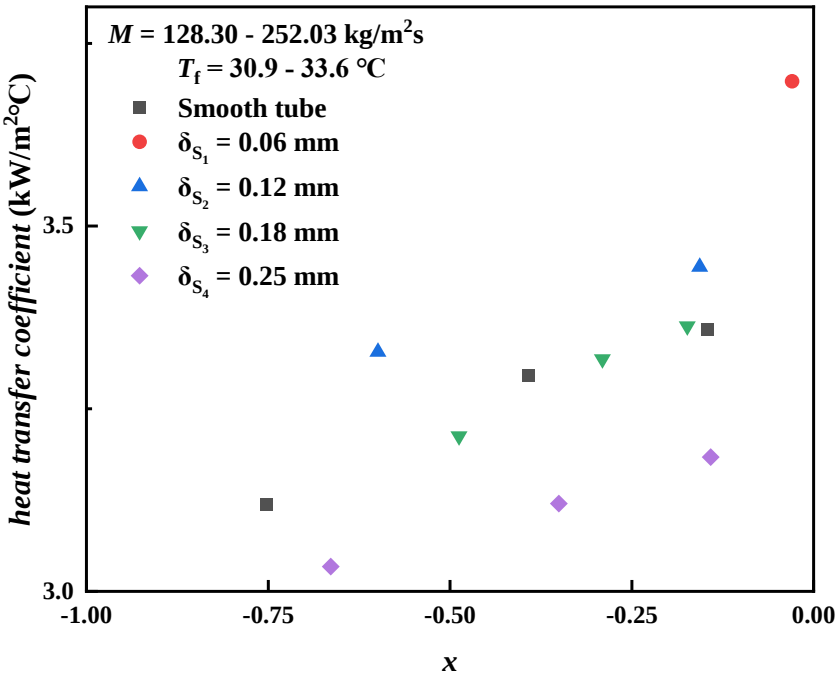

(a)

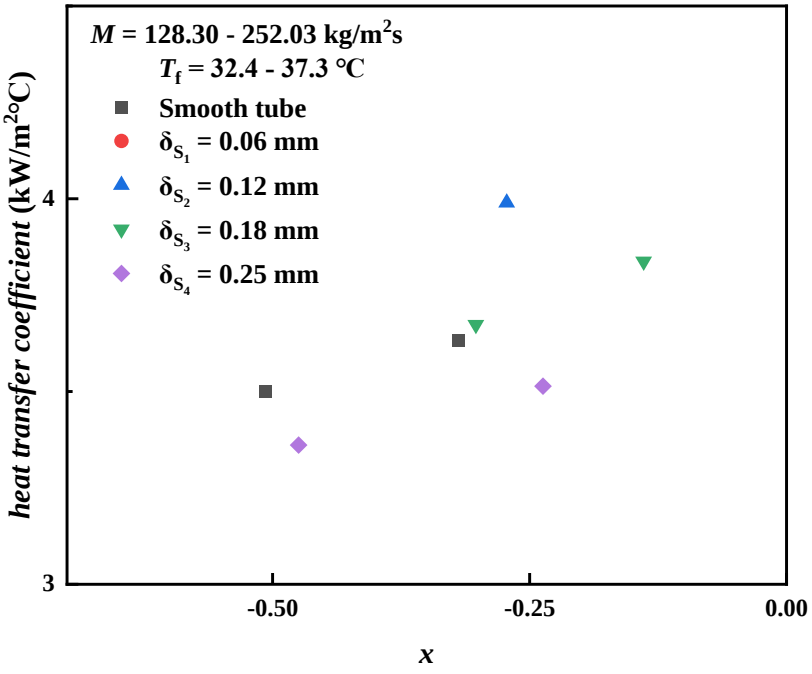

(b)

Figure 9. The relationship between vapor quality and heat transfer coefficient under subcooled boiling.

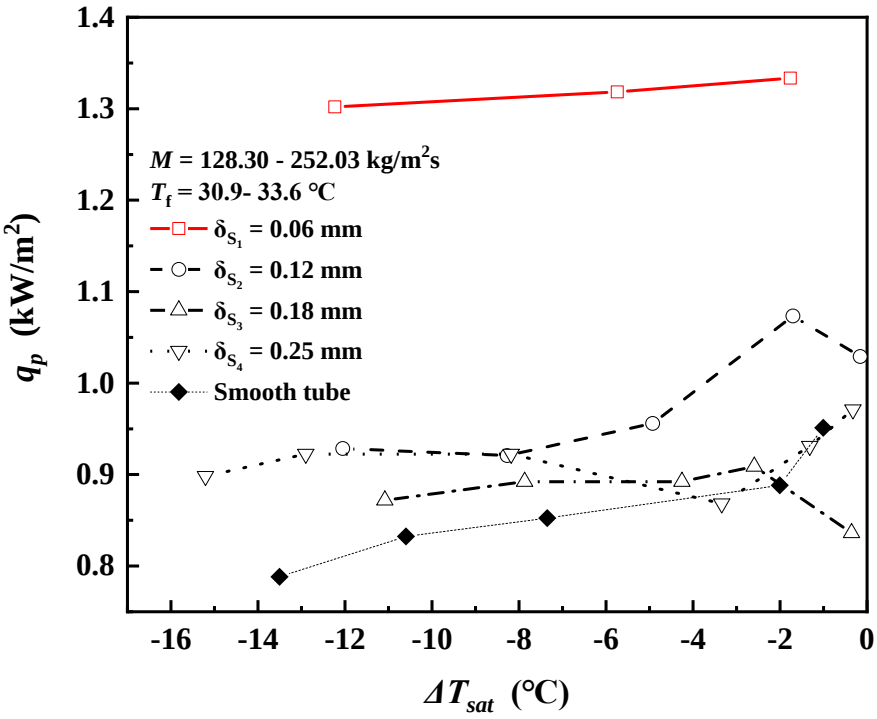

(a)

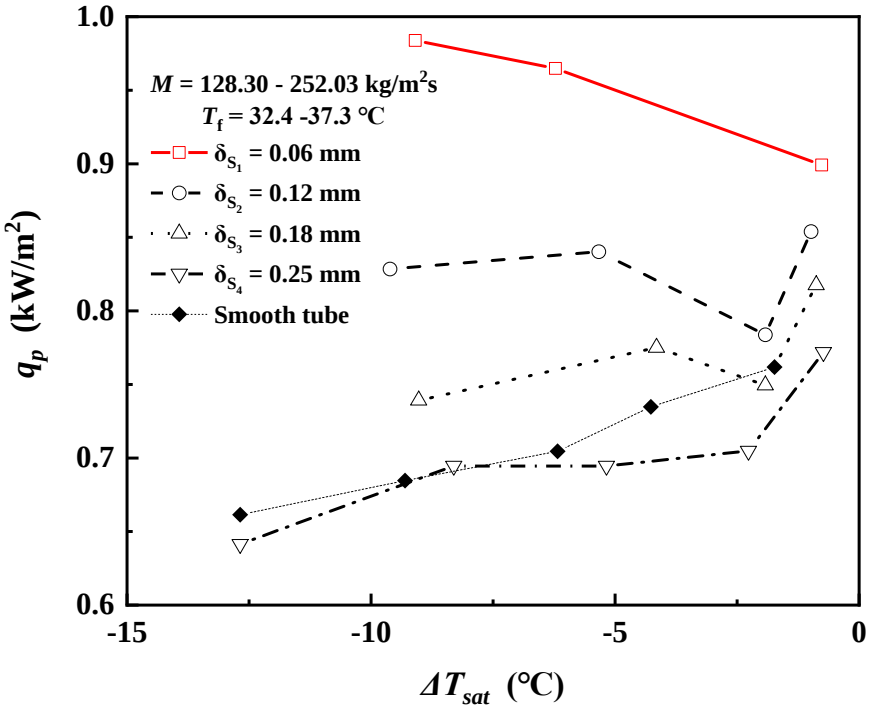

(b)

Figure 10. The relationship between the thickness of the sintered layer and the superheat required for boiling.

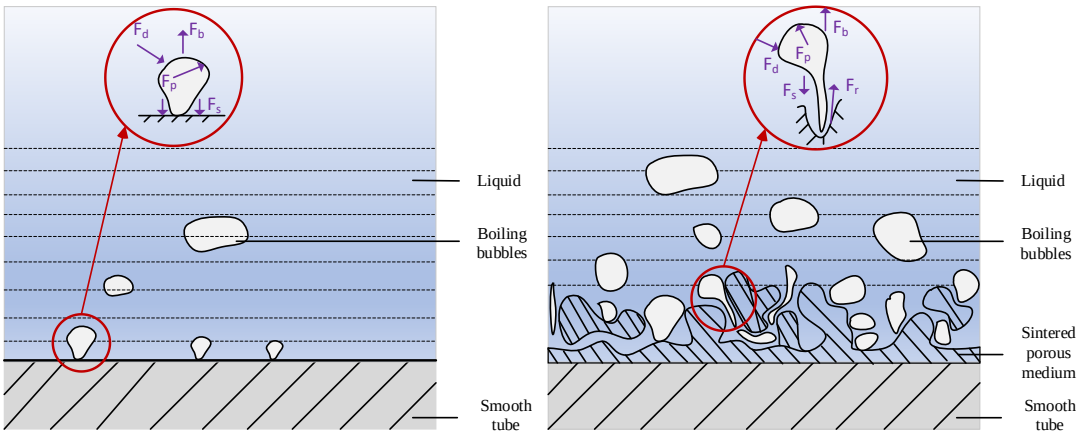

(a) Smooth surface.

(b) Thinner porous layer.

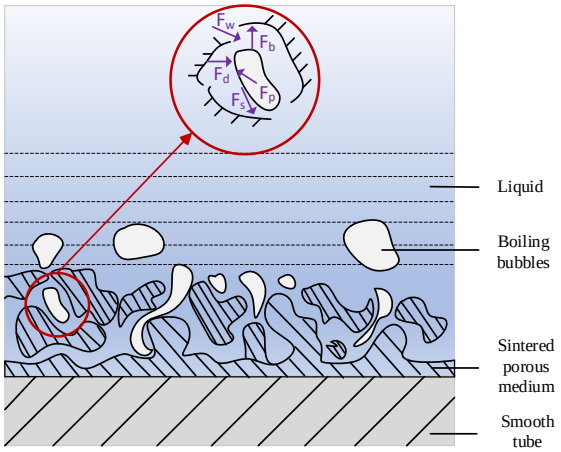

(c) Thicker porous layer.

Figure 11. Bubble growth and detachment force analysis.

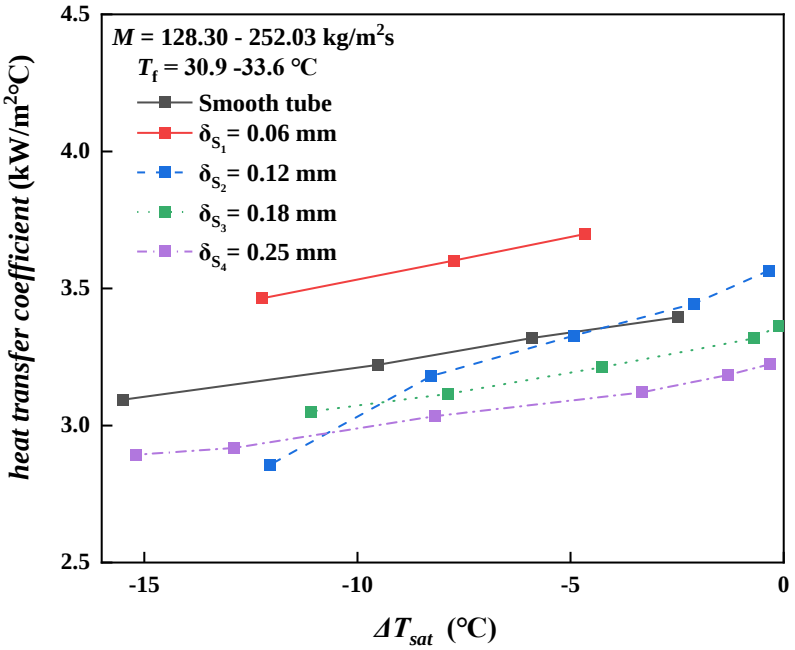

(a)

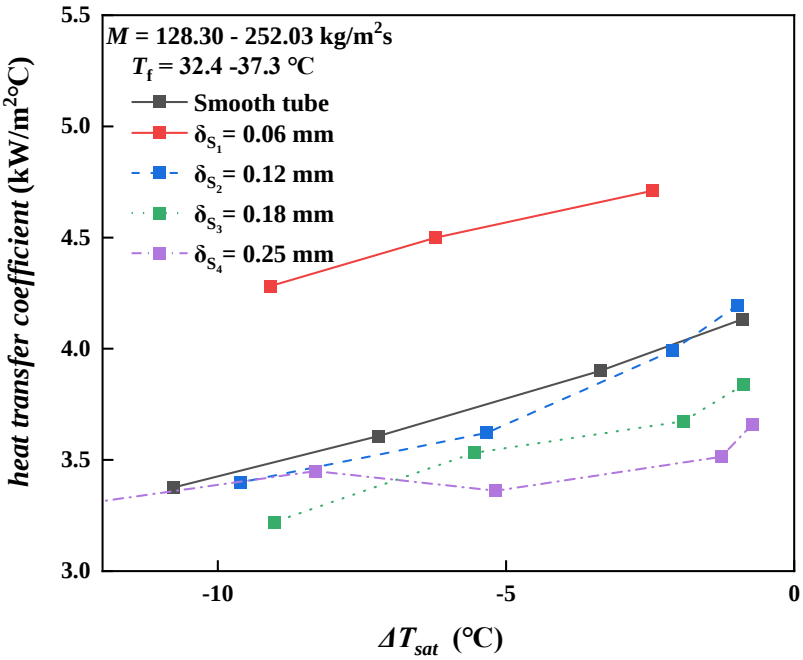

(b)

Figure 12. The relationship between the subcooled boiling heat transfer coefficient vs. superheat degree.

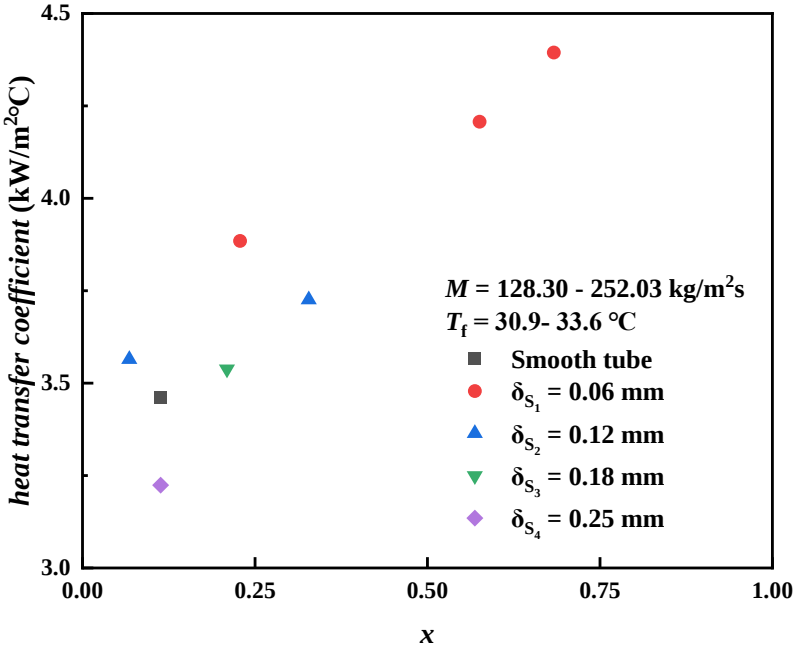

(a)

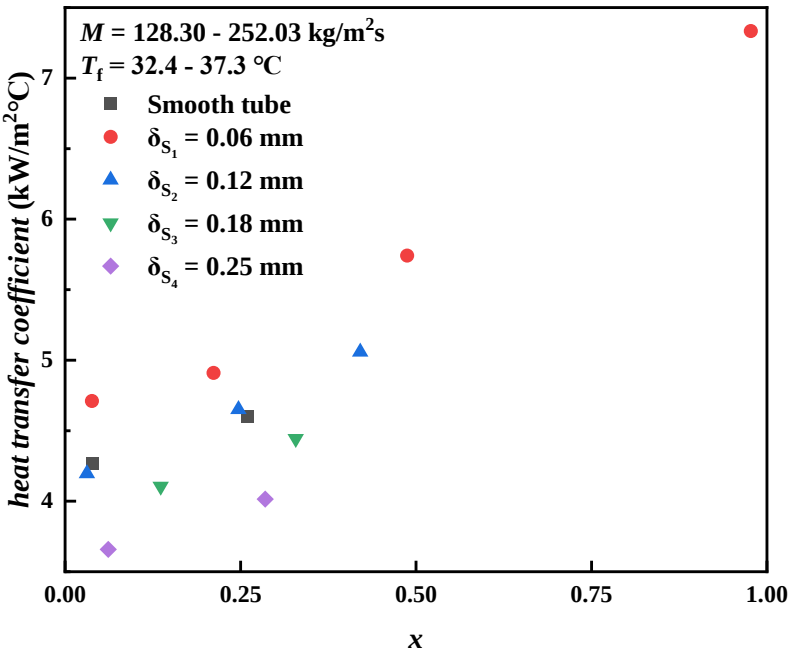

(b)

Figure 13. The relationship between saturated flow boiling heat transfer coefficient vs vapor quality.

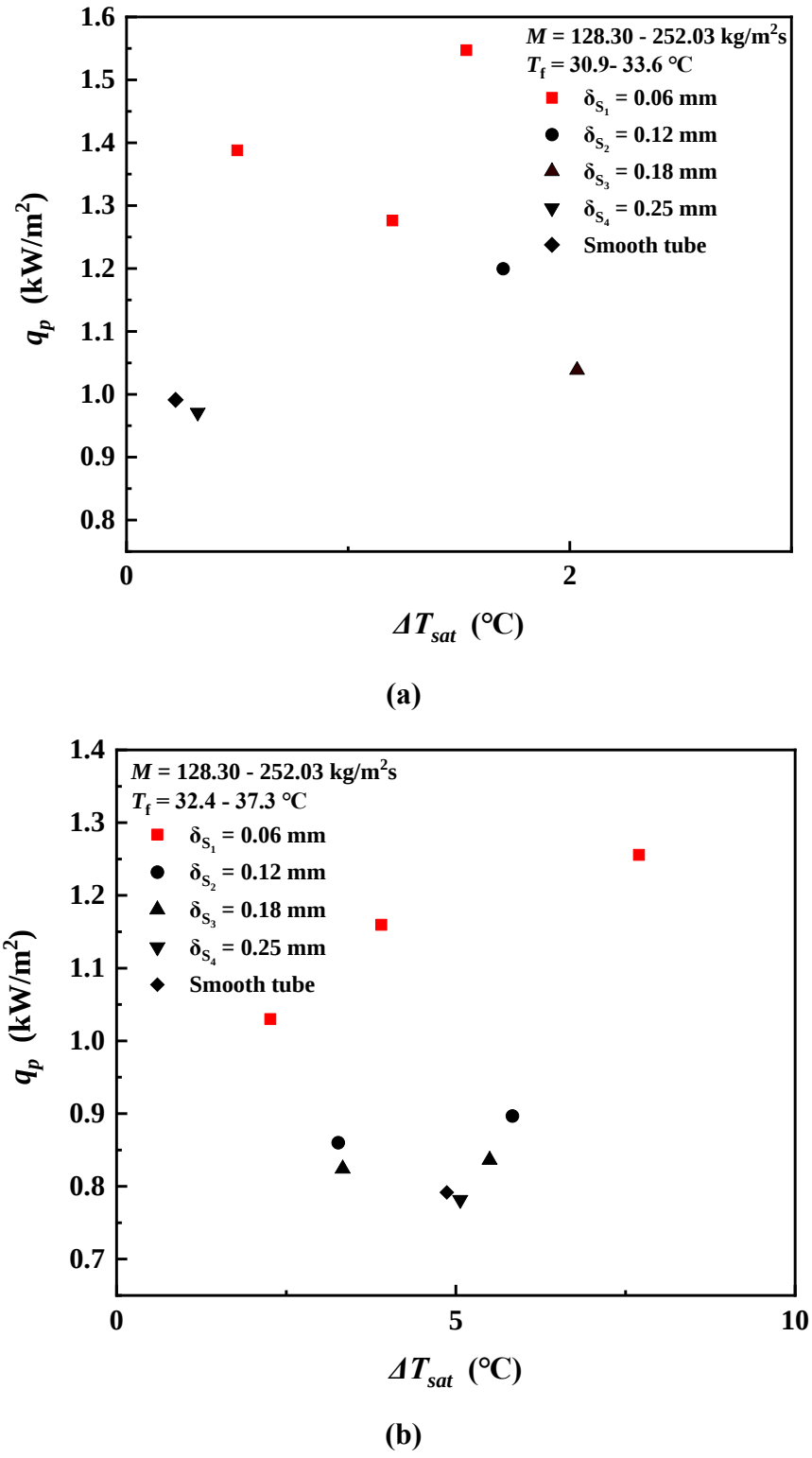

Figure 14. Variation of the heat flux vs. superheat degree under saturated flow boiling.

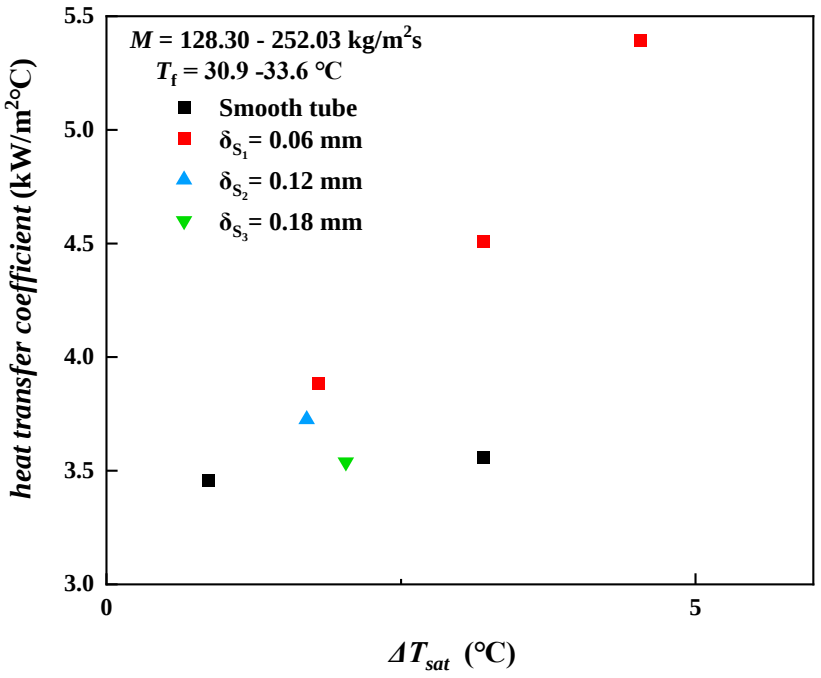

(a)

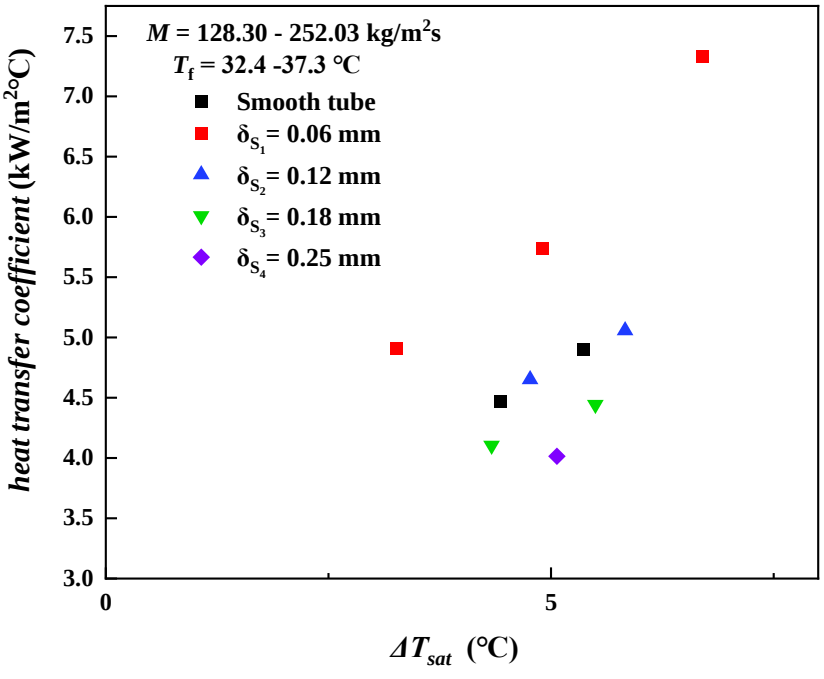

(b)

Figure 15. Variation of saturated flow boiling heat transfer vs. superheat degree.

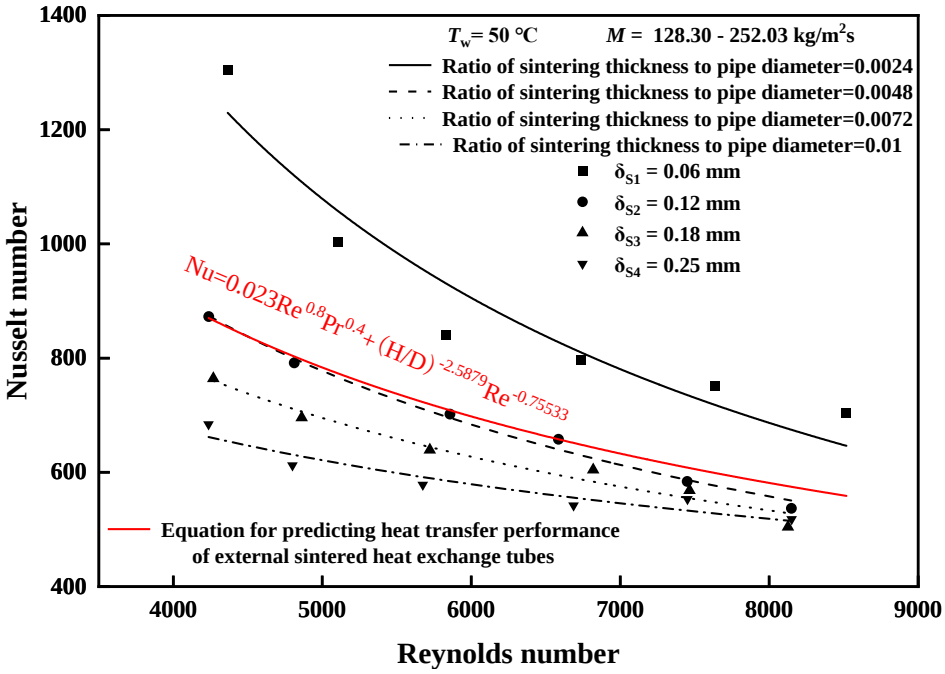

Figure 16. Variation of the Nusselt number with the Reynolds number.